BAU Journal - Science and Technology

Volume 4 | Issue 2
ISSN: 2959-331X

Article 4

June 2023

ROBUST AND PARALLEL SEGMENTATION MODEL (RPSM) FOR EARLY DETECTION OF SKIN CANCER DISEASE USING HETEROGENEOUS DISTRIBUTIONS

Nancy Zreika
Department of Computer Sciences, Faculty of Science, Beirut Arab University, Lebanon, nancy_zreika@hotmail.com

Ali El-Zaart
Department of Computer Sciences, Faculty of Science, Beirut Arab University, Lebanon, elzaart@bau.edu.lb

Abdallah El Chakik
Department of Computer Sciences, Faculty of Science, Beirut Arab University, Lebanon, a.alshakik@bau.edu.lb

1. INTRODUCTION

Skin cancer is the most common type of cancers in humans [38]. There are two types of skin cancer; melanoma and non-melanoma. Melanoma is more dangerous and can be fatal if not treated. A non-melanoma tumor is a benign tumor and it is unable to spread. To rule out skin cancer, five main ABCDE properties (Asymmetry, Border, Color, Diameter, and Evolving) in the lesion, are considered [39]. Several segmentation techniques have been proposed to measure and analyze these properties but none of them is able to give the optimal result for every image. For that purpose, an efficient and robust system that detects skin cancer details is needed.

Image segmentation is an important preparatory process, in image processing. It consists of partitioning an image into several segments to make it more significant and easier to analyze [16]. In each segment, pixels should be homogeneous in terms of level of intensities, to obtain an optimum segmentation [15]. One of the easiest image segmentation approaches is Thresholding [16]. In their simplest case, bi-level thresholding methods consist in finding one optimum threshold value T for the pixel's intensity. The pixels are divided into two classes based on their intensity values; bigger than T belongs to the first class, and the rest belongs to the second class. Usually, one class is for the background region, and another for the object region of the image [15]. However, sometimes, one threshold is not sufficient to extract the objects of interest from multi-classes images, and two thresholds and more would be required. Most of the skin cancer images are composed of three main classes: cancerous lesion, new growth or precancerous lesion and the normal skin. Then, applying bi-level segmentation on these images, will result in a loss of information.

MCET approach is the most popular thresholding technique, because of its accuracy, efficiency and ease of implementation [17]. It consists of minimizing the distance between the original image and the thresholded in order to estimate the optimum threshold [15]. In addition, the accuracy of MCET results will be certainly affected by the number of image classes and the prediction of distribution type applied on each class. In other words, the histogram of an image is a combination of different statistical distributions, and the prediction of this combination plays an essential role in detecting the best thresholds. One drawback of the MCET technique is that its complexity growths when the number of threshold points increases, which makes this method a time-consuming one [41].

In this paper, a novel multilevel segmentation model based on heterogeneous MCET is designed. The designed model uses a combination of statistical distributions: Gamma, Gaussian and lognormal. Additionally, a parallel processing method is implemented to boost the performance of the proposed model and to minimize its computational cost in term of time while detecting the optimum thresholds of the image.

This research study deals with:

(1) Constructing a multilevel segmentation model using a heterogeneous MCET based on Gamma, Gaussian and lognormal distributions.
(2) Optimizing the objective function of cross entropy to obtain the optimum threshold points.
(3) Developing a parallel processing algorithm to enhance the performance of the suggested model in term of time consuming.
(4) Significant simulation using two benchmark skin cancer datasets: ISIC and PH2, to test the efficiency of the suggested model.

2. RELATED WORK

MCET technique has been the simplest technique used to estimate the optimum threshold. It was used widely and has been known for its robustness in improving the segmentation of different types of images. Li et al. suggested a thresholding model based on MCET to extract the optimum threshold value. Brink et al. in [17] improved Li's version by suggesting a new method based on a true symmetric cross entropy. Pal assumed that each pixel in the segmented image is modeled by a statistical distribution, and he used Poisson distribution to estimate an accurate threshold [16]. Chakraborty et al. [42] developed a multilevel thresholding model using particle swarm optimization and based on MCET technique to find the best threshold. Zreika et al. [3] improved the work of Pal by applying a bimodal segmentation based on homogeneous cross

entropy technique. They obtained promising experimental results on skin cancer images by using Gamma distribution. A hybrid and bi-level cross entropy thresholding model, is developed by Zreika et al. [4], for optimum thresholding of Alzheimer's Disease images.

Most of the previous proposed segmentation models are bi-level thresholding models. However, a wide range of images are multilevel one and require more than one threshold to detect their objects of interest. Moreover, the previous proposed models apply a single distribution type to detect the threshold points even though each level of the image follows a different type of distributions. Additionally, the computational complexity which growths seriously with thresholding levels, is ignored [6]. Accordingly, two main contributions are underlined in this paper: (1) developing an precise multimodal MCET-based segmentation model for skin cancer detection by using the three combined statistical distributions (Gamma, Gaussian and Lognormal) and (2) parallelizing the implemented model to reduce its computational time.

3. IMAGE SEGMENTATION AND THRESHOLDING TECHNIQUE

To extract the objects from the background, we used Cross Entropy Thresholding Technique. Thresholding techniques consist of detecting the best thresholds that extract the objects of interest into an image, based on several properties like intensity, texture, color, etc. [9,10]. These techniques are classified into two categories: Bimodal segmentation and Multimodal segmentation. Bimodal segmentation divides the image into two regions: one for the object region and another for the background region, while multimodal segmentation consists of partitioning the image into several regions. In this paper, we use a multimodal segmentation because skin cancer images are multilevel images and one threshold is not sufficient to extract their objects of interest.

3.1 Bimodal Segmentation

The bimodal technique consists of one threshold that segments the image into two classes: class 1 and class 2.

Figure 1 shows a bimodal histogram where the threshold T* divides the region into two classes.

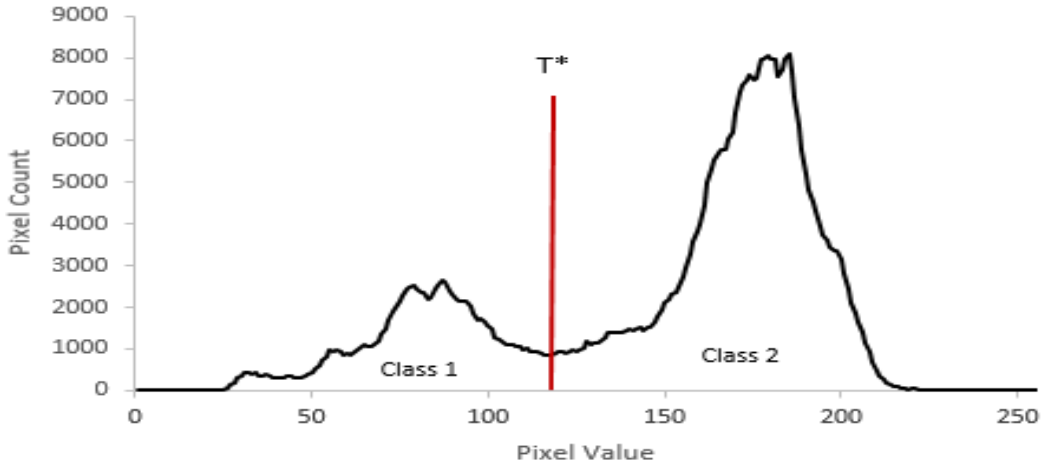

Fig.1: A histogram with 2 classes separated by 1 threshold line.

Bimodal segmented image is defined as follows:

$$I_t(x,y) = \begin{cases} \mu_1(0, T^*), & I_o(x,y) < T^* \\ \mu_2(T^*, 255), & I_o(x,y) \geq T^* \end{cases} \quad (1)$$

$I_o(x,y)$ represents the original image, $I_t(x,y)$ is the image intensity (pixel value) used to represent the segmented image and T* ranges between [0, 255].

μ_1 and μ_2 represent the means of class 1 and class 2 respectively.

To distinguish a dark object image from the light background, a threshold T* would lie in the valley of a bimodal histogram in which the foreground object can be extracted by comparing pixels with the threshold T*.

If $I_o(x, y) < T^*$, then the pixel (x, y) is belonging to the object class, otherwise, it belongs to the background class.

3.2 Multimodal Segmentation

The multimodal technique divides the image into a number of separate regions, using several thresholds. In this paper, we used to segment the image to three regions where two thresholds are required.

Figure 1 shows a multimodal histogram of an image where T_1^* and T_2^* are the optimal thresholds that divide the image histogram to three regions: class 1, class 2 and class 3.

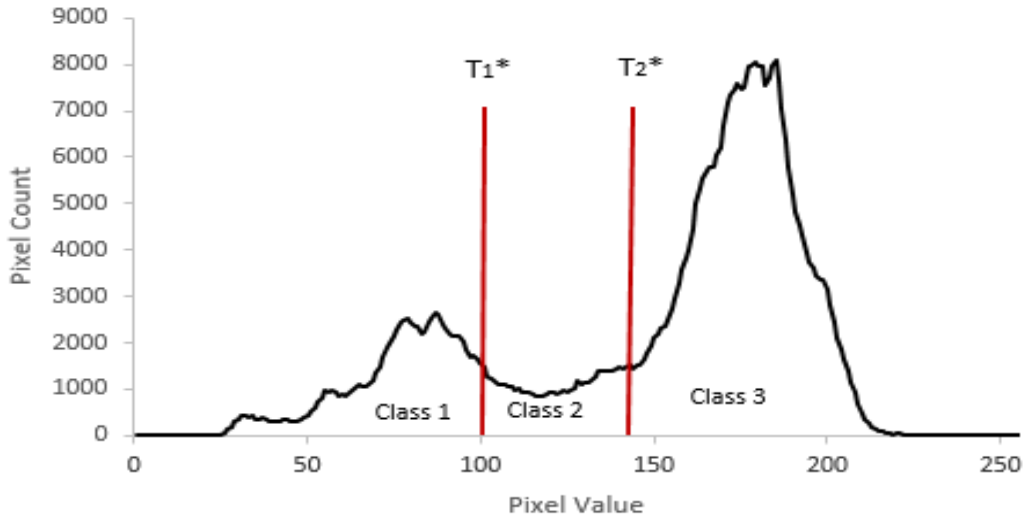

Fig.2: A histogram with 3 classes separated by 2 threshold lines.

Multimodal segmented image is represented as follows:

$$I_t(x,y) = \begin{cases} \mu_1(0, T_1^*), & I_o(x,y) < T_1^* \\ \mu_2(T_1^*, T_2^*), & T_1^* \le I_o(x,y) < T_2^* \\ \dots & \\ \mu_k(T_{k-1}^*, T_k^*), & T_{k-1}^* \le I_o(x,y) < T_k^* \\ \dots & \\ \mu_m(T_{m-1}^*, 255), & I_o(x,y) \ge T_{m-1}^* \end{cases} \quad (2)$$

$\mu_1, \mu_2, \dots, \mu_m$ are the means of the *m* extracted classes separated by *m-1* thresholds respectively.

The multiple regions are extracted by comparing image pixels with the various thresholds ranging between 0 and 255.

4. CROSS ENTROPY THRESHOLDING AND STATISTICAL DISTRIBUTIONS

4.1. Cross Entropy Thresholding

The cross entropy between two different sources of information F and G, indicates the information of the theoretical distance between these sources [16]. Cross entropy is measured by Kullback using the following formula [15]:

$$D(F, G) = \sum_{i=0}^{L-1} f_i \cdot \log\left(\frac{f_i}{g_i}\right) \quad (3)$$

Where f_i and g_i are the probabilistic distributions of *F* and *G*; *L* states the number of information values; *D (F, G)* measures the distance between *F* and *G*.

Lee and Li applied the cross entropy defined by Kullback, to estimate the threshold.

Brink and Pendock assumed that the objective function of Kullback is non-symmetric and they proposed a true symmetric cross entropy as it follows [16]:

$$D(F, G) = \sum_{i=0}^{L-1} f_i \cdot log\frac{f_i}{g_i} + \sum_{i=0}^{L-1} g_i \cdot log\frac{g_i}{f_i} \quad (4)$$

Consider that we have two classes in the image: region1 and region2.

The cross entropy $D_1(t)$ between region1 of the source F and region1 of the source G, is as it follows:

$$D_1(t) = D(F_1, G_1) = \sum_{i=0}^{t} f_i^1 \, log\left(\frac{f_i^1}{g_i^1}\right) + \sum_{i=0}^{t} g_i^1 \, log\left(\frac{g_i^1}{f_i^1}\right) \quad (5)$$

The cross entropy $D_2(t)$ between region2 of the source F and region2 of the source G, is as it follows:

$$D_2(t) = D(F_2, G_2) = \sum_{i=t+1}^{L-1} f_i^2 \, log\left(\frac{f_i^2}{g_i^2}\right) + \sum_{i=t+1}^{L-1} g_i^2 \, log\left(\frac{g_i^2}{f_i^2}\right) \quad (6)$$

Thus, the total cross entropy remains:

$$D(t) = D_1(t) + D_2(t) \quad (7)$$

Both Lee and Brink assumed that each pixel in region 1 and region 2 of the thresholded image should be equal to the average of pixels' value respectively in the corresponding region of the original image [16].

Pal used the symmetric version defined by Brink, but he assumed that each pixel in the segmented image is modeled by a statistical distribution [16]. He applied a bimodal segmentation based on homogeneous distribution.

In this study, we developed the cross entropy defined by Pal, by applying a multimodal segmentation based on heterogeneous distribution.

4.2.Minimum Cross Entropy Thresholding

The minimization of the cross entropy forces the total intensity in the thresholded image to be identical to that of the original image in both region 1 and region 2. The more similar the distribution of two variables, the smaller cross entropy is, and vice versa.

Then, to obtain an optimum threshold, *MCET* minimizes the total cross entropy *D(t)* between *F* and *G*.

$$T^* = arg\ min_t\ (D(t)) \quad (8)$$

4.3.Statistical Distributions

A histogram displays probabilistic information of pixels' distribution in an image. Pixels' distribution in a histogram can have one of the two shapes: symmetric and non-symmetric. Gaussian performs well with symmetric distribution, but leads to poor segmentation results when the distribution is non-symmetric [19]; whereas Lognormal and Gamma distributions characterize both shapes. In image segmentation, a good prediction of the distribution type describing the pixels of each image class, leads to the optimum thresholding. Next, we introduce the functions for the probabilistic distributions used in our proposed methodology.

4.3.1. Gaussian Distribution

Gaussian distribution is described by the following function [35,36]:

$$f(x,\mu,\sigma) = \frac{1}{\sigma\sqrt{2\pi}} e^{\frac{-1}{2}\left(\frac{x-\mu}{\sigma}\right)^2} \quad (9)$$

Where x is the pixel's intensity level,

μ is the mean defined as: $\mu = \frac{\sum_{i=0}^{L} i.h(i)}{\sum_{i=0}^{L} h(i)}$ (10)

and σ is the standard deviation defined as: $\sigma^2 = \frac{\sum_{i=0}^{L}(\mathrm{i}-\mu)^2.h(i)}{\sum_{i=0}^{L} h(i)}$ (11)

And, the distribution means of the object and the background and their standard deviations using Gaussian distribution, are respectively:

$$\mu_1 = \frac{\sum_{\mathrm{i}=0}^{\mathrm{t}-1} \mathrm{i.h(i)}}{\sum_{\mathrm{i}=0}^{\mathrm{t}-1} \mathrm{h(i)}} \quad (12)$$

$$\mu_2 = \frac{\sum_{\mathrm{i}=t}^{\mathrm{L}} \mathrm{i.h(i)}}{\sum_{\mathrm{i}=\mathrm{t}}^{\mathrm{L}} \mathrm{h(i)}} \quad (13)$$

$$\sigma_1^2 = \frac{\sum_{\mathrm{i}=0}^{t-1}(\mathrm{i}-\mu)^2.\mathrm{h(i)}}{\sum_{\mathrm{i}=0}^{t-1} \mathrm{h(i)}} \quad (14)$$

And $$\sigma_2^2 = \frac{\sum_{\mathrm{i}=t}^{\mathrm{L}}(\mathrm{i}-\mu)^2.\mathrm{h(i)}}{\sum_{\mathrm{i}=t}^{\mathrm{L}} \mathrm{h(i)}} \quad (15)$$

Gaussian distribution estimates only a symmetric shape of histogram [3].

4.3.2. Lognormal Distribution

Lognormal distribution, whose logarithm is normally distributed, is used to display symmetric and moderate positively skewed data. This is a continuous statistical distribution and its density function is defined as [35,36]:

$$f(x,\mu,\sigma) = \frac{1}{x\sigma\sqrt{2\pi}} e^{\frac{-1}{2}\left(\frac{lnx-\mu}{\sigma}\right)^2} \quad (16)$$

Where the mean is defined as:

$$\mu = \frac{\sum_{i=0}^{L} ln(i).h(i)}{\sum_{i=0}^{L} h(i)} \quad (17)$$

And the standard deviation is estimated as:

$$\sigma^2 = \frac{\sum_{i=0}^{L}(ln(i)-\mu)^2.h(i)}{\sum_{i=0}^{L} h(i)} \quad (18)$$

Therefore, the distribution means of the object and the background and their standard deviations using Lognormal distribution, are respectively

$$\mu_1 = \frac{\sum_{\mathrm{i}=0}^{\mathrm{t}-1} \ln(\mathrm{i}).\mathrm{h(i)}}{\sum_{\mathrm{i}=0}^{\mathrm{t}-1} \mathrm{h(i)}} \quad (19)$$

$$\mu_2 = \frac{\sum_{\mathrm{i}=\mathrm{t}}^{\mathrm{L}} \ln(\mathrm{i}).\mathrm{h(i)}}{\sum_{\mathrm{i}=\mathrm{t}}^{\mathrm{L}} \mathrm{h(i)}} \quad (20)$$

$$\sigma_1^2 = \frac{\sum_{\mathrm{i}=0}^{\mathrm{t}-1}(\ln(\mathrm{i})-\mu)^2.\mathrm{h(i)}}{\sum_{\mathrm{i}=0}^{\mathrm{t}-1} \mathrm{h(i)}} \quad (21)$$

$$\sigma_2^2 = \frac{\sum_{\mathrm{i}=\mathrm{t}}^{\mathrm{L}}(\ln(\mathrm{i})-\mu)^2.\mathrm{h(i)}}{\sum_{\mathrm{i}=\mathrm{t}}^{\mathrm{L}} \mathrm{h(i)}} \quad (22)$$

Log-normal distribution is symmetric. As σ rises, Lognormal distribution skews to the right [3].

4.3.3. Gamma Distribution:

Gamma Distribution is a continuous probability distribution of two parameters μ and N, where μ is the mean and N is the parameter shape. The shape of Gamma distribution function goes from symmetric to asymmetric by varying the parameter shape N. Gamma distribution is used to estimate symmetric and non-symmetric data. Gamma function is given by [35,36]:

$$f(x,\mu,N) = \frac{2q}{\mu}\frac{N^N}{\Gamma(N)}\left(\frac{qx}{\mu}\right)^{2N-1}e^{-N\left(\frac{qx}{\mu}\right)^2} \quad (23)$$

Where $q = \frac{\Gamma(N+0.5)}{\sqrt{N}\,\Gamma(N)}$ (24)

and $\mu^2 = \frac{\sum_{i=0}^{L} h(i).i^2.q^2}{\sum_{i=0}^{L} h(i)}$ (25)

And, the distribution means of the object and the background using Gamma distribution, are respectively

$$\mu_1^2 = \frac{\sum_{i=0}^{t-1} h(i).i^2.q^2}{\sum_{i=0}^{t-1} h(i)} \quad (26)$$

$$\mu_2^2 = \frac{\sum_{i=t}^{L} h(i).i^2.q^2}{\sum_{i=t}^{L} h(i)} \quad (27)$$

The curve is skewed to right when N=1, and tends to be symmetric when N increases [3].

5. PERFORMANCE METRICS

Several performance metrics are frequently used to evaluate the segmentation accuracy, such as Image Uniformity (UN) and Region Contrast (RC) [24,26].

UN describes region homogeneity in the thresholded image, which is proportional to the variances of two consecutive classes. For a given threshold *t*, UN is defined as follows:

$$UN(t) = 1 - \frac{\sigma_1^2(t)+\sigma_2^2(t)}{C} \quad (28)$$

$\sigma_1^2(t)$ and $\sigma_2^2(t)$ represent respectively the variances of two consecutive regions in the image, and

$$C = \frac{(g_{max}-g_{min})^2}{2} \quad (29)$$

g_{max} represents the maximum grey level value, while g_{min} represents the minimum grey level value in the original image, and they range between 0 and 255.

Region Contrast (RC) identifies the presence of high contrast across adjacent regions in the thresholded image. For a given t, the region contrast is defined as [24]:

$$RC(t) = \frac{|\mu_1(t)-\mu_2(t)|}{\mu_1(t)+\mu_2(t)} \quad (30)$$

Where μ_1 and μ_2 are the averages of the grey level values of 2 consecutive classes.

The arithmetic average of UN and RC is:

$$AVG = \frac{UN+RC}{2} \quad (31)$$

The values of UN, RC and their average AVG range between 0 and 1. A value of 1 indicates a perfect segmentation while a value of 0 indicates a bad segmentation. The higher the average of UN and RC, the better the quality of the segmentation.

6. RPSM MODEL FORMULATION

6.1. Modeling the Image Segmentation Problem

RPSM is an entropy-based model, designed to find the optimum threshold t^* by minimizing the total cross entropy between the original image and the thresholded one. Different combinations of statistical distributions have been used and performance metrics are applied to compare the results and detect the best combination that leads to optimal threshold t*. Therefore, this model is a nondeterministic polynomial (NP)-hard optimization problem having the cross entropy function D(t) as an objective function and subject to the quality constraints UN(t) and RC(t).

Solving this problem aims to find the best thresholded outputs through minimizing D(t) and maximizing UN(t) and RC(t) using respectively the Equations (28) and (30).

Note that t* ranges between [0, 255].

6.2. RPSM Model Formulation

We have proposed in this work, a multimodal segmentation based on MCET-PAL method by using heterogeneous distributions. The proposed method considers that the image is composed of multiple classes, where each class is described by one statistical distribution. Therefore, the means $\mu_1(t)$, $\mu_2(t)$, …. and $\mu_m(t)$ are estimated from different distributions according to the assessed region. Hence, the histogram of the image is written as it follows:

$$h(x)= P_1 * dist_1(x, \mu_1(t)) + P_2 * dist_2(x, \mu_2(t)) + \ldots\ldots + P_m * dist_m(x, \mu_m(t)) \quad (32)$$

such that $dist1(x, \mu_1(t))$ is the first distribution and $dist2(x, \mu_2(t))$ is the second distribution,…., and $dist_m(x, \mu_m(t))$ is the distribution numbered m; and P_1, P_2, …., P_m are the probability for each distribution respectively.

To test our proposed method, we limit the number of classes to three, and we apply one type of distribution on each class. We use all the combinations between Gamma, Gaussian and Lognormal distribution.

6.3. Multimodal Cross Entropy Thresholding

Threshold selection techniques are classified into 2 categories: bimodal and multimodal thresholding [27]. While some histograms tend to be bimodal and a single threshold is sufficient to extract the foreground from its background, other histograms may require multiple thresholds that help to separate their objects of interest.

In multimodal thresholding technique, an image has *m* classes segmented by *m-1* thresholds. Next is a description of the cross entropy *D (F, G)* between two probabilistic distribution F and G assuming that F represents the original image *(I)* and G represents the resultant thresholded image *(I_t)*, based on multimodal thresholding technique [10,27,31].

Assume T= $\{t_1, t_2, t_3, t_4, \ldots, t_{m-1}\}$ is a set of threshold values, where $t_0 \; t_1 \; t_2 \; \ldots \; t_{m-1} \; t_m$, t_0 and t_m *L-1*.

$$D(F, G) = D_1(t_1) + D_2(t_2) + \ldots\ldots + D_m(t_m) \quad (33)$$

$$= D(F_1, G_1) + D(F_2, G_2) + \cdots + D(F_m, G_m) \quad (34)$$

$$= \sum_{i=t_0}^{t_1} f_i^1 \log\left(\frac{f_i^1}{g_i^1}\right) + \sum_{i=t_0}^{t_1} g_i^1 \log\left(\frac{g_i^1}{f_i^1}\right) + \sum_{i=t_1+1}^{t_2} f_i^2 \log\left(\frac{f_i^2}{g_i^2}\right) + \sum_{i=t_1+1}^{t_2} g_i^2 \log\left(\frac{g_i^2}{f_i^2}\right) + \ldots\ldots + \sum_{i=t_{m-1}}^{t_m} f_i^m \log\left(\frac{f_i^m}{g_i^m}\right) + \sum_{i=t_{m-1}}^{t_m} g_i^m \log\left(\frac{g_i^m}{f_i^m}\right) \quad (35)$$

Where f_i and g_i are two probabilistic distributions of a grey level respectively in *I* and I_t, and *L* states to the number of grey levels.

f_i^1 , f_i^2, …., f_i^m are the probabilities of occurrence of grey level *i* in *(I)* and are estimated as follows:

$$f_i^1 = \frac{h(i)}{\sum_{i=0}^{t_1-1} h(i)} \quad (36), \qquad f_i^2 = \frac{h(i)}{\sum_{i=t_1}^{t_2-1} h(i)} \quad (37), \ldots\ldots\ldots, \qquad f_i^m = \frac{h(i)}{\sum_{i=t_{m-1}}^{t_L} h(i)} \quad (38)$$

Where *h(i)* represents the histogram of grey level *i*.

g_i^1, g_i^2, …, g_i^m are estimated by using respectively one of the statistical distributions mentioned in *Section 4.3.*

Multimodal thresholding method is an extension of the bimodal thresholding one since we apply a bimodal thresholding technique on each two consecutive classes of the histogram [27,32].

7. SOLVING THE OPTIMIZATION PROBLEM AND RPSM ALGORITHM

7.1 Workflow Design of RPSM Algorithm

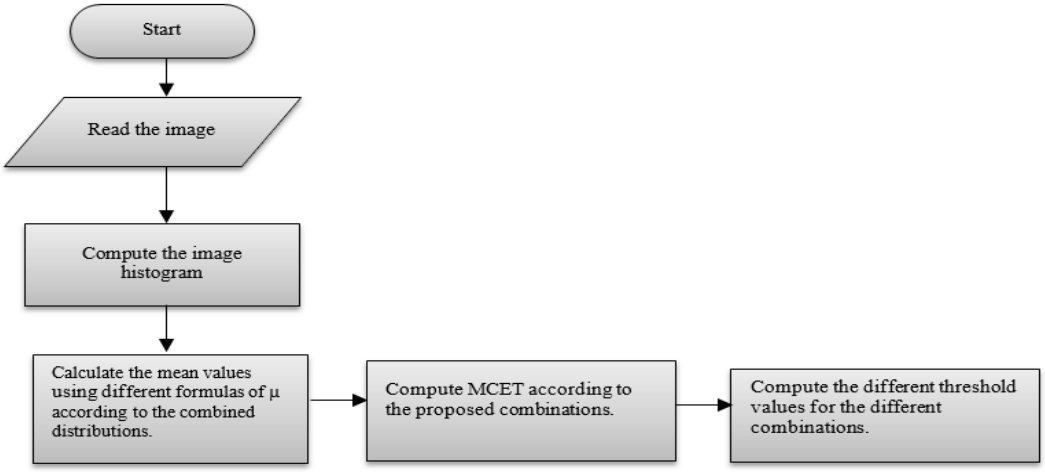

7.2 Bimodal Heterogeneous MCET-PAL Based Algorithm

The algorithm reads the original grey level image *I (x, y)* (line 1), computes its histogram *h(i)* (line 2), and selects one of the heterogeneous thresholding methods as inputs. At the end, it returns the value of the threshold (t*), that optimizes MCET and minimizes the distance between the original image and the resultant image.

1. Input: *I(x, y)* and the number of modes *m* (m=2 in the case of bimodal segmentation)
2. Compute *h(i)* of *I (x, y)*, where *i=0…255.*
3. for each value of *t=1, ..., 255*
   - 3.1 Compute $\mu_1(t)$ and $\mu_2(t)$ using equations (10), (17) or (25) according to the selected heterogeneous distributions (one type of statistical distribution is applied on the first region and another type is applied on the second region).
   - 3.2 Compute the probability distributions of region1 and region2 in the thresholded image g_i^1 and g_i^2 using equations (9), (16) or (23) according to the selected heterogeneous distributions
   - 3.3 Compute $D_1(t)$ and $D_2(t)$ using equations (5) and (6).
   - 3.4 Compute the total cross entropy *D(t)* using equation (7).
   - 3.5 Compute the minimum distance and the corresponding threshold

     If (*min* > *D(t)*)

     {

     min = *D(t)* ;

     }
4. Output: optimal threshold: *t**

7.3 Multimodal Heterogeneous MCET-PAL Based Algorithm

The multimodal algorithm reads the image and the number of modes (classes) (line 1), computes its histogram (line 2), and computes the initial values of threshold $t_0^1, t_0^2, \ldots, t_0^{m-1}$ using k-mean algorithm (line 3). In order to find the new value of threshold t_{new}^k (line 4), multimodal algorithm applies the bimodal MCET-PAL based algorithm on each two consecutive modes in the multimodal histogram. These two modes are starting from t_{k-1} and ending at t_k. For k=1,2, …, m-1.

Then, it compares the two threshold t_0 and t_{new}.

If $|t_0 - t_{new}| < \varepsilon$ then optimal threshold values $T^* = \{t_1^*, t_2^*, t_3^*, \ldots\ldots, t_{m-1}^*\}$ are reached (line 5).

Else Assign $t_0 \leftarrow t_{new}$ and Go to line 4.

1. Inputs: *I (x, y)* and number of modes *m* (The value of m is 3 or more according to the number classes in the thresholded image)
2. Compute histogram *h(i)* of the image where *i=0,1, 2, …. ,255.*
3. Compute initial threshold values $\{t_0^1, t_0^2, \ldots, t_0^{m-1}\}$ using k-mean algorithm.
4. Compute new threshold value t_{new}^k using the previous bimodal algorithm.
5. If $|t_0 - t_{new}| < \varepsilon$ then optimum threshold values $T^* \leftarrow \{t_1^*, t_2^*, t_3^*, \ldots\ldots, t_{m-1}^*\}$ are reached.

   Else

   Assign $t_0 \leftarrow t_{new}$

   Go to step 4.

To detect the best threshold, the computational complexity, using a homogenous distribution, is $O(L^2)$ [43]. However, under heterogeneous distribution scenarios, detecting the best threshold could be extensive and time consuming. Therefore, for n thresholding problem, the RPSM computational complexity will be $O(L^{n+1})$. For that purpose, we propose to use a parallelized processing technology, with the aim to consume properly the computational resources and to reduce the processing time.

8. PARALLEL PROCESSING AND PARALLELIZED RPSM ALGORITHM

Parallel processing is a method used to perform complex tasks and complex computations simultaneously. Large problems can be divided into smaller ones, which can then be solved in parallel and independently. Results are combined subsequently, once completed.

Parallel processing consists of running two or more central processing units (CPUs) to handle, in parallel, separate parts of an overall task, in order to overcome the processing time problem.

Due to the recursive programming and the exhaustive search to find the optimum thresholds, MCET computation is known as a complex process and a time consuming one [44]. Consequently, the proposed RPSM algorithm has been parallelized among two Core i5 processors with four concurrent threads, to get over the problem of its computational time.

Nevertheless, to profit from the benefit of the multithreading technique while designing parallel algorithms, we should apply the data dependency constraint. In fact, one of the fundamental conditions to implement a multithreading algorithm is that its parallelized sub-tasks shouldn't have dependent data [45].

Data dependency: Consider $Segm_i$ and $Segm_j$ are two program segments running concurrently in a system S.

Let $Segm_i$ have Inp_i and Out_i as the input and output variables, respectively$_i$, and $Segm_j$ have Inp_j and Out_j as the input and output variables, respectively. Hence to run the two program segments concurrently, the following conditions should be fulfilled:

$$Inp_i \cap Out_j = \emptyset$$
$$Inpj \cap Out_i = \emptyset$$
$$Out_i \cap Outj = \emptyset$$

The applied parallel processing technology can be useful to any application that fulfils the data dependency constraints. Particularly, we parallelized our system by implementing a parallel computing of the different thresholds (T*) using the corresponding obtained MCET objective functions.

Parallel processing RPSM implementation

for j = 1 : 255 do

Parallel computing of the thresholds (T*) according to the statistical combination used

End for

With the above parallelization, we can accelerate the proposed RPSM algorithm up to p times using a multiprocessor machine.

The efficacy of the proposed RPSM is evaluated by using C++ language and OpenCV (Open Source Computer Vision Library) with 2.5 GHz Intel(R) Core(TM) i5-3210 machine of 6 GB RAM. The processors feature two cores with four concurrent threads. We have developed a multithreaded implementation using C++ **Thread** function that allows the implementation of parallel functions on a multicore computing platform.

9. EXPERIMENTAL RESULTS AND DISCUSSION

In this work, we compared our proposed multimodal heterogeneous combinations together and with the classical multimodal techniques based on a single distribution. The performance is tested on two benchmark skin cancer datasets PH2 and ISIC 2017. PH2 dataset [13] is developed in Portugal by the Dermatology Department of Pedro Hispano Hospital and contains 200 melanocytic lesions. ISIC 2017 dataset, is maintained by the International Society for Digital Imaging of the Skin [30], and encloses 2000 dermoscopic images of skin lesions collected from several worldwide clinical centers [21].

We evaluated the performance of the proposed methods, by recording the performance metrics UN1, RC1, UN2 and RC2, where UN1 and RC1 are respectively the region homogeneity and the region contrast across region 1 and region 2 in the thresholded image, and UN2 and RC2 are respectively the region homogeneity and the region contrast across region 2 and region 3 in the thresholded image. Then we calculated UN and RC, which are UN1 and UN2 average, and RC1 and RC2 average, respectively.

The experiment was performed on 200 melanocytic lesions images from PH2 dataset, and 200 dermoscopic skin lesions images selected randomly from ISIC 2017 dataset.

A sample of the testing results is shown in Figure 2, Figure 3, Figure 4, Figure 5, and Figure 6. Each figure contains an original image, a chart showing the histogram of the image along with 2 vertical lines representing the value of the optimum thresholds T1 and T2, the performance measures UN1, RC1 and AVG1 corresponding to threshold T1 and UN2, RC2 and AVG2 corresponding to T2, and the thresholded image resulting from multilevel segmentation based on the best found combination Gamma-Lognormal-Gaussian. For example, in figure 2-(c), the optimum threshold T1 that extracts the first region from the second one is 119 and the corresponding performance measures are as follows: UN1=0.955332, RC1=0.397369, AVG1=0.676351. As well, the optimum threshold T2 that extracts the second region from the

third one is 147 and the corresponding performance measures are: UN2=0.956943, RC2=0.351116, AVG2=0.654030. Also, UN=0.956138 represents the average of UN1 and UN2 and RC= 0.374243 belongs to the average of RC1 and RC2. Finally, the global performance measure average of the whole image is AVG=0.665190 which represents UN and RC average.

In Figure 2-(d), three levels appear in the segmented image: the dark region refers to the cancerous lesion, the grey region refers to the new growth or precancerous lesion that will be infected in the future, and the white region which refers to the normal skin. In this figure, the grey level is reducing due to the high contrast (RC2=0.351116) between the cancerous lesion and the normal skin in the original image. While in Figure 3, the grey level is more significant due to the low contrast (RC2=0.284438) between the infected region and the normal skin.

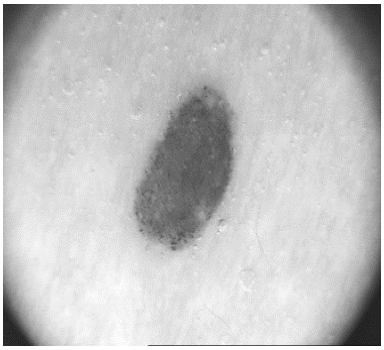

(a)

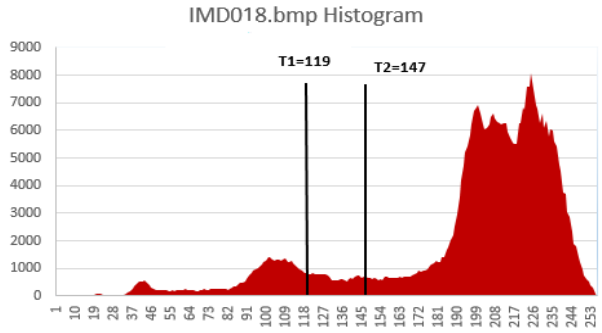

(b)

T1=119, UN1=0.955332, RC1=0.397369, AVG1=0.676351

T2=147, UN2=0.956943, RC2=0.351116, AVG2=0.654030

UN = 0.956138, RC = 0.374243, AVG (UN, RC) = 0.665190

(c)

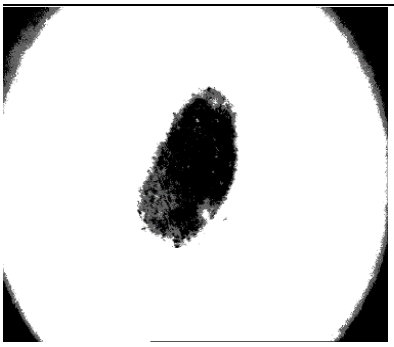

(d)

Fig.2: (a)original image (IMD018), (b)the histogram of the image, (c) the thresholds value (T1 and T2) with their performance measures, (d) the thresholded image resulting from multilevel segmentation based on (Gamma-LogNormal-Gaussian) combination.

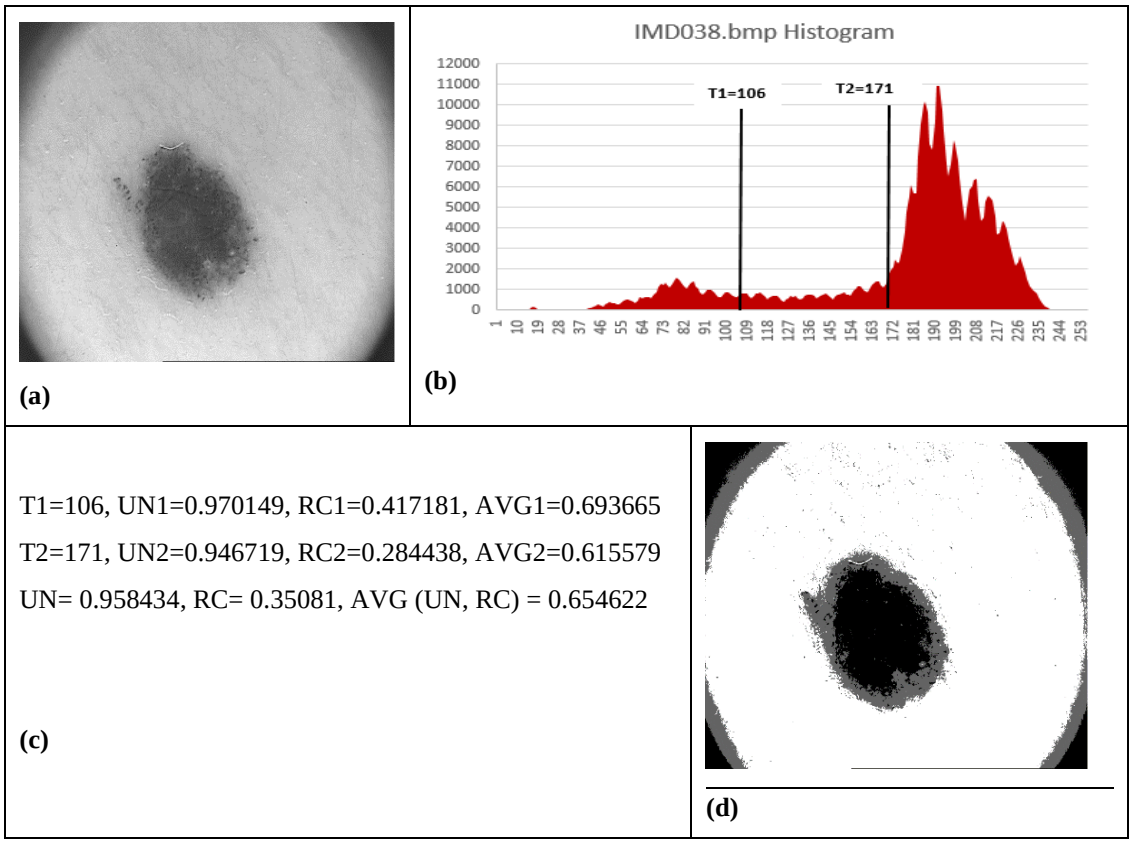

Fig.3: (a) original image (IMD038), (b) the histogram of the image, (c) the thresholds value (T1 and T2) with their performance measures, (d) the thresholded image resulting from multilevel segmentation based on (Gamma-LogNormal-Gaussian) combination.

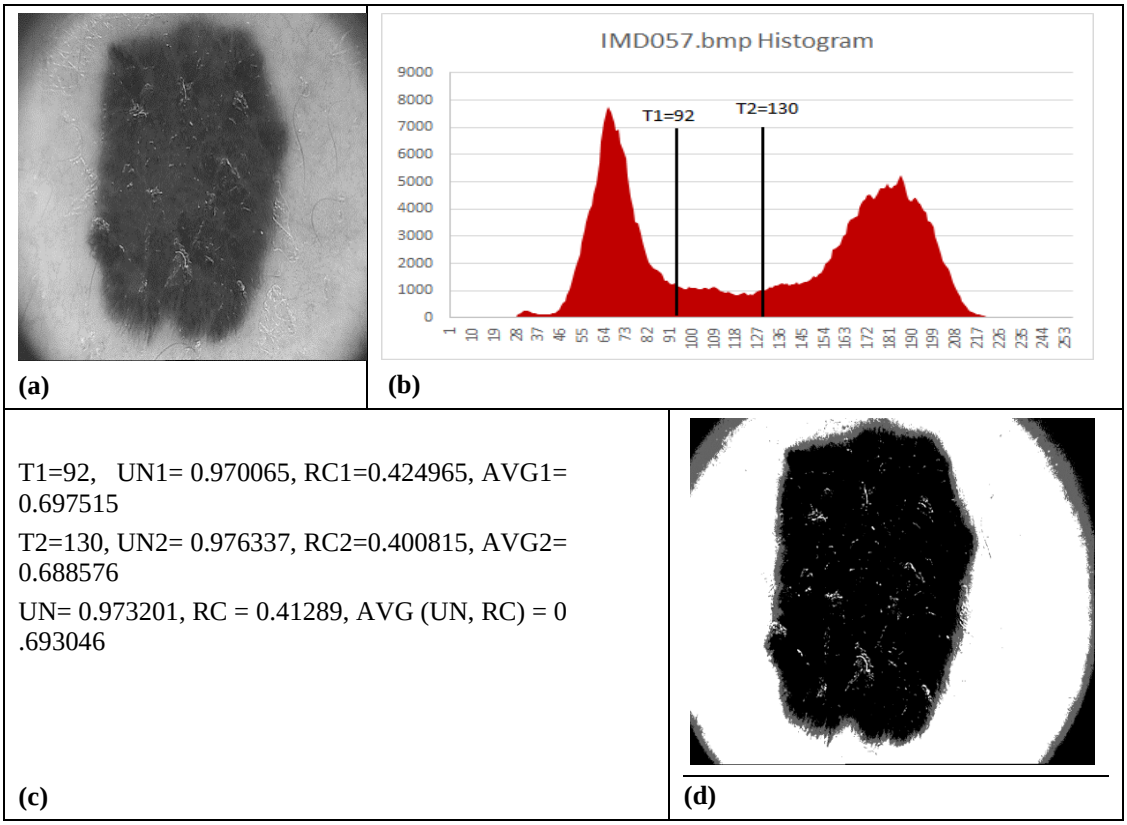

Fig.4: (a) original image (IMD057), (b) the histogram of the image, (c) the thresholds value (T1 and T2) with their performance measures, (d) the thresholded image resulting from multilevel segmentation based on (Gamma-LogNormal-Gaussian) combination.

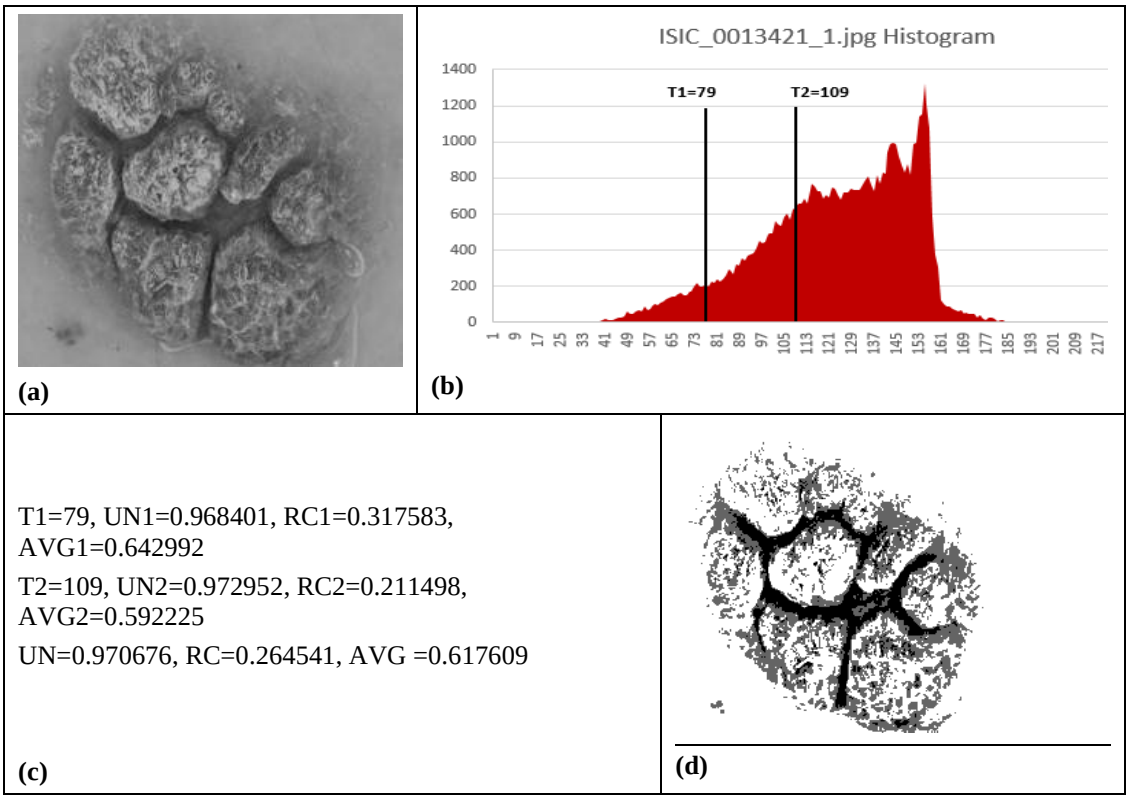

Fig.5: (a)original image (ISIC_0013421_1), (b)the histogram of the image, (c) the thresholds value (T1 and T2) with their performance measures, (d) the thresholded image resulting from multilevel segmentation based on (Gamma-LogNormal-Gaussian) combination.

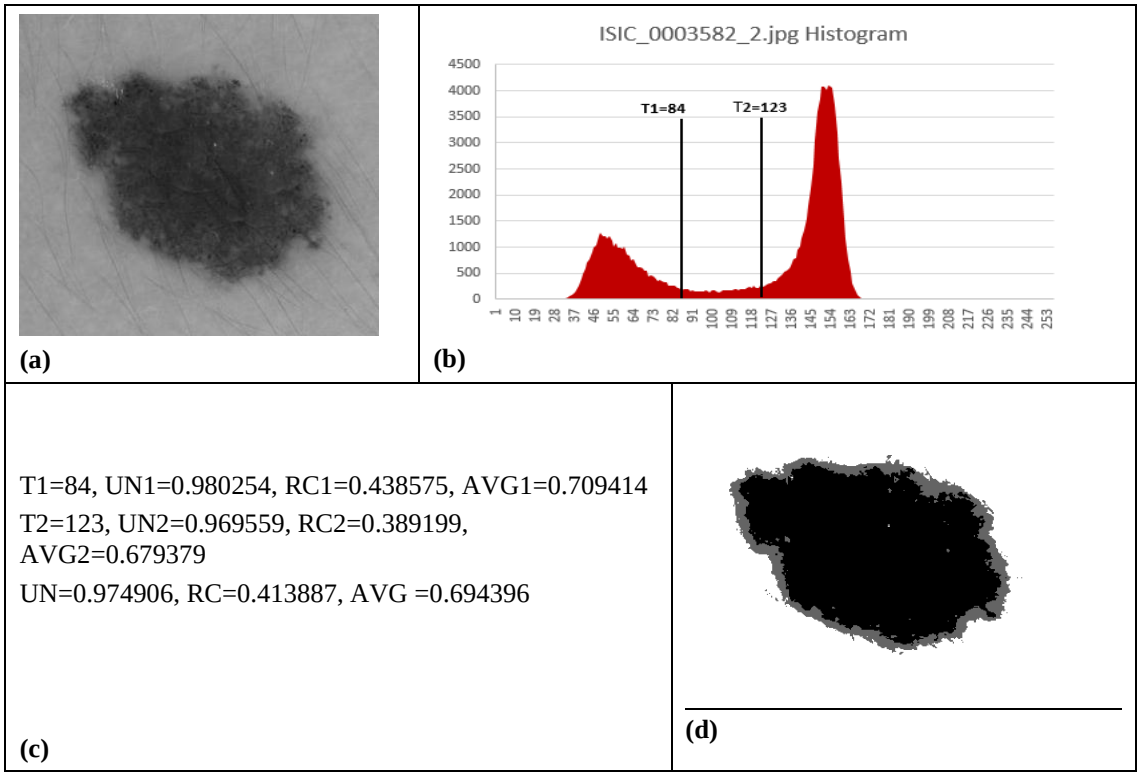

Fig.6: (a) original image (ISIC_0003582_2), (b) the histogram of the image, (c) the thresholds value (T1 and T2) with their performance measures, (d) the thresholded image resulting from multilevel segmentation based on (Gamma-LogNormal-Gaussian) combination.

Table 1 illustrates an exhaustive comparison of various statistical distributions combinations used in our proposed methodology. The table shows the percentage of best segmented lesions for each method according to UN, RC, and their average AVG. In PH2 Dataset, the first column (%UN) represents the percentage of images showing better UN average performance measure according to each combination, and the second column (%RC) represents the percentage of images showing better RC average performance measure according to each combination. For instance, according to the methodology (Gamma-Lognormal-Gaussian), 34 images out of 200 images of PH2 dataset show better UN performance measure, 162 images out of 200 images show better RC performance measure, and 154 images out of 200 images show better AVG performance measure; which explains correspondingly the percentage values 17%, 81% and 77% that belongs respectively to UN, RC and AVG obtained in table 1. Therefore, in PH2 dataset, 77% of the tested images show better UN and RC average performance measure with Gamma-Lognormal-Gaussian combination. The other 23% is distributed over the remaining combinations. As well, in ISIC2017 dataset, 74% of the tested images show better UN and RC average performance measure with Gamma-Lognormal-Gaussian combination, and the other 26% is distributed over the remaining combinations. Accordingly, this could conclude that Gamma-Lognormal-Gaussian combination reached the optimum result with an average of 75.5% compared to other homogeneous and heterogeneous combinations, which can validate that skin cancer histograms mostly followed Gamma, lognormal and Gaussian distribution at their start, mid and endpoints, respectively. Furthermore, homogeneous methods face significant problems to detect the optimal thresholds as shown in our experimental results.

Table 1: Results of the proposed multilevel segmentation method based on homogeneous and heterogeneous distributions and using PH2 and ISIC2017 Datasets.

	PH2 Dataset			ISIC 2017 Dataset				
Methodology	**%UN**	**%RC**	**%AVG**	**%UN**	**%RC**	**%AVG**	**Two datasets Average**	**Rank**
Gaussian-Gaussian-	0.5	0.0	0.0	1.0	0.0	0.0	0.0	15
Lognormal-Lognormal-	2.0	1.0	1.0	3.0	0.0	1.0	1.0	9
Gamma-Gamma-Gamma	3.0	2.0	2.0	5.0	1.0	3.0	2.5	3
Gamma-Lognormal-	17.0	81.0	77.0	22.0	78.0	74.0	75.5	1
Gamma-Gaussian-	57.0	8.0	10.5	39.0	11.0	9.0	9.8	2
Gaussian-Lognormal-	1.0	0.5	0.5	2.0	1.0	1.0	0.8	10
Gaussian-Gamma-	2.0	1.0	0.5	3.0	0.5	1.0	0.8	10
Lognormal-Gaussian-	1.0	0.5	0.5	4.0	0.0	2.0	1.3	7
Lognormal-Gamma-	0.5	2.0	2.0	1.0	3.0	3.0	2.5	3
Gamma-Gamma-Gaussian	3.0	1.0	3.0	1.0	2.0	1.0	2.0	5
Gamma-Gamma-	2.0	1.0	1.0	3.0	1.0	2.0	1.5	6
Gamma-Gaussian-Gaussian	3.0	0.0	0.5	1.0	0.0	0.0	0.3	13
Gamma-Lognormal-	2.0	1.0	0.5	3.0	1.0	2.0	1.3	7
Lognormal-Lognormal-	0.5	0.0	0.0	1.0	0.5	0.0	0.0	15
Lognormal-Lognormal-	0.0	0.5	0.5	0.5	0.0	0.0	0.3	13
Lognormal-Gamma-	2.0	0.5	0.5	3.0	1.0	1.0	0.8	10
Lognormal-Gaussian-	0.0	0.0	0.0	1.0	0.0	0.0	0.0	15
Gaussian-Gaussian-Gamma	1.0	0.0	0.0	1.0	0.0	0.0	0.0	15
Gaussian-Gaussian-	0.0	0.0	0.0	0.0	0.0	0.0	0.0	15
Gaussian-Gamma-Gamma	0.0	0.0	0.0	0.5	0.0	0.0	0.0	15
Gaussian-Lognormal-	0.0	0.0	0.0	0.5	0.0	0.0	0.0	15
Gaussian-Lognormal-	1.0	0.0	0.0	2.0	0.0	0.0	0.0	15
Gaussian-Gamma-Gaussian	0.5	0.0	0.0	1.0	0.0	0.0	0.0	15
Lognormal-Gaussian-	0.0	0.0	0.0	0.0	0.0	0.0	0.0	15

Lognormal-Gamma-	0.0	0.0	0.0	0.0	0.0	0.0	0.0	15
Gamma-Gaussian-Gamma	0.5	0.0	0.0	0.5	0.0	0.0	0.0	15
Gamma-Lognormal-	0.5	0.0	0.0	1.0	0.0	0.0	0.0	15

Parallel processing proficiency The proposed RPSM is formulated to execute program on parallel cores, and aims to reduce the processing time and to provide optimum proficiency. This is clearly denoted by the total computing time taken by the CPU to complete the segmentation using a parallel processing segmentation model. Table 2 shows a comparison of the computing time given in seconds between sequential method and our proposed parallel computing method. Accordingly, it can be observed that the processing time performance under parallel computing get over the sequential method with an average of 53.03%. This will validate the high performance and the consistency of our proposed parallel computing model.

Table 2: Performance improvement using RPSM parallel processing model

Dataset Name	Sequential method (secs)	Parallel computing method (secs)	Saving Time (%)
PH2 Dataset	7854.88	3682.96	53.11
ISIC 2017 Dataset	7635.35	3593.33	52.94

The chart of figure 10 represents the average of UN and RC measures for 28 randomly selected images from both PH2 and ISIC2017 datasets. Each curve of the chart corresponds to the following combinations: Gaussian-Gaussian-Gaussian, Lognormal-Lognormal-Lognormal, Gamma-Gamma-Gamma, and Gamma-Lognormal-Gaussian, respectively. As can be seen in this chart, the combination Gamma-Lognormal-Gaussian performs better in UN and RC average than the other 3 homogeneous benchmark methods. Therefore, we can conclude that the heterogeneous method using Gamma-Lognormal-Gaussian distributions results in better segmentation of skin cancer images than using the 3 well-known homogeneous benchmark methods Gamma, Gaussian and Lognormal.

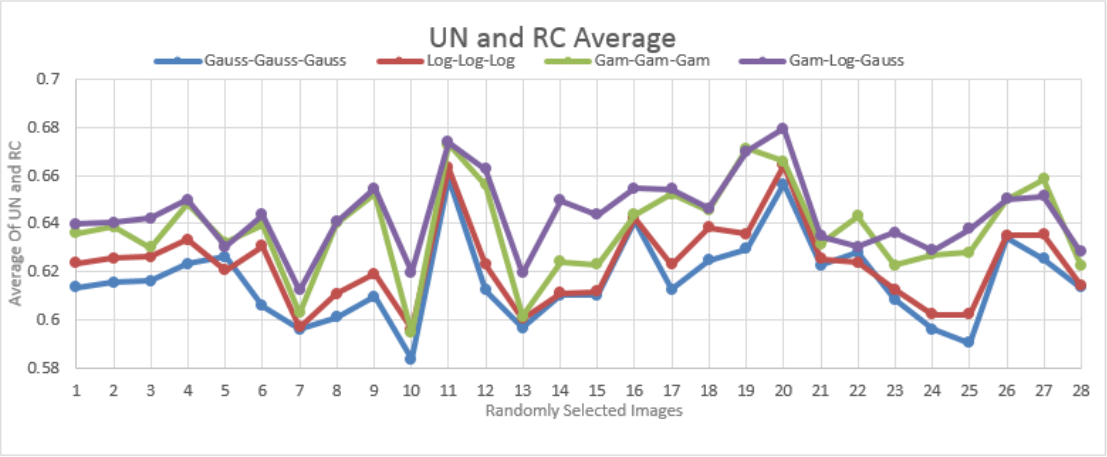

Fig.10: Performance metrics measurement comparing the proposed multilevel (Gamma-Lognormal-Gaussian) method accuracy with the 3 homogeneous benchmark methods.

10. CONCLUSION AND FUTURE WORK

In this paper, we have improved the segmentation of skin cancer and melanoma images by using a combination of various statistical distributions (i.e. Gamma, Lognormal and Gaussian). This approach was implemented to fit multimodal images and to improve the prediction of cancerous lesions progression. The performance of our suggested model was tested using two benchmark of skin cancer datasets. As shown in our experiments, the suggested methodology using the combination (Gamma-Lognormal-Gaussian) empirically outperformed the other heterogeneous methods and the three well known classical homogeneous methods. Additionally, the proposed RPSM model used a parallel processing technology to reduce the computing time of segmentation and enhance its performance.

We aim to expand this work to cover different types of image processing applications like Alzheimer's disease images, radar images, and satellite images. We further aim to study and extend new performance metric measures that can better detect the quality and the accuracy of the segmentation.

REFERENCES

- Hala Al-Shamlan, Ali El-Zaart, Breast Cancer Computer aided Diagnosis (CAD) System, Proceedings of the International Conference on Image Processing, Computer Vision, and Pattern Recognition (IPCV), 2011.
- Sandhya, G.; Giri, K.; Savitri, S. A novel approach for the detection of tumor in MR images of the brain and its classification via
- independent. Imaging Med. 2017, 9, 33–44.
- N. A. Zreika, A. El-Zaart, A. Al Shakik, (2021), "An Improvement Of Cross Entropy Thresholding For Skin Cancer Detection", ISSN:2706-784X, © BAU Journal - Beirut Arab University, Vol: 2, Issue: 2, Page:2, Lebanon .
- Nancy A. Zreika, A. El-Zaart, A. Al Shakik, " A Hybrid Cross Entropy Thresholding for Early Alzheimer's Disease Detection ", International Journal of Computing and Digital Systems, ISSN (2210-142X) , 2021.
- Oliva D, Abd Elaziz M, Hinojosa S. Multilevel thresholding for image segmentation based on metaheuristic algorithms. Metaheuristic Algorithms for image Segmentation: Theory and Applications; Cham: Springer; 2019: 59-69.
- Amani Al-Ajlan, Ali El-Zaart, Image segmentation using minimum cross-entropy thresholding, 2009 IEEE International Conference on Systems, Man and Cybernetics, 1776-178, 2009.
- Horng M-H. Multilevel thresholding selection based on the artificial bee colony algorithm for image segmentation. Expert Syst Appl. 2011;38(11):13785-13791.
- Ayala HVH, dos Santos FM, Mariani VC, dos Santos Coelho L. Image thresholding segmentation based on a novel beta differential evolution approach. Expert Syst Appl. 2015;42(4):2136-2142.
- Horng MH. A multilevel image thresholding using the honey bee mating optimization. Appl Math Comput. 2010;215(9):3302-3310. doi:10.1016/j.amc.2009.10.018.
- Li, Jiafu, et al. "A multilevel color image thresholding scheme based on minimum cross entropy and alternating direction method of multipliers." *Optik* 183 (2019): 30-37.
- Mishra, Nabin K., et al. "Automatic lesion border selection in dermoscopy images using morphology and color features." *Skin Research and Technology* (2019).
- Ferrari R.J., Rangayyan R.M., BORGES R.A, FRERE A.F. (2004): "Segmentation of the fibro-glandular disc in mammograms using Gaussian mixture modeling", Med. Biol. Eng. Comput., 42, pp. 378-87
- PH^2Database,https://www.fc.up.pt/addi/ph2%database.html, Accessed November 2017
- C.H.Li and P K S Tam (1998), "An iterative algorithm for minimum cross entropy thresholding", Pattern Recognition Vol 19, pp 771-776
- S. Kullback (1959), Information Theory and Statistics. Wiley, New York.
- Pal, N. (1996), "On Minimum cross entropy thresholding," Pattern Recognition Letter, vol. 29 no. 4, pp. 575–580.

- A. Brink, and N. Pendock, “Minimum Cross-entropy Threshold Selection,” Pattern Recognition Letter - Elsevier, vol. 29, no. 1, 1996, pp. 179-188.
- Hui-Lan Luo, Wei-Wang, and Jing-LI (2010), “A new method for image segmentation based on integration technique,” in MVHI, Kaifeng, China, pp. 342–345.
- G.McPherson,”Statistics in scientific investigation: its basis, application and interpretation”, Springer-Verlag,1990.
- C. Forbes, et al., "Statsitical Distributions" 4th edition, John wiley & Sons, 2011.
- Codella N, Rotemberg V, Tschandl P, Celebi ME, Dusza S, Gutman D, Helba B, Kalloo A, Liopyris K, Marchetti M, Kittler H. Skin lesion analysis toward melanoma detection 2018: a challenge hosted by the international skin imaging collaboration (isic). arXiv preprint arXiv:1902.03368: 2019.
- ŞENGÜR, I. TÜRKOĞLU and M. İNCE (2006), "A Comparative Study On Entropic Thresholding Methods" Journal of Electrical & Electronics Engineering, vol.6, no. 2, pp. 183-188.
- Sun, Hao, Xianqiang Yang, and Huijun Gao. "A spatially constrained shifted asymmetric Laplace mixture model for the grayscale image segmentation." *Neurocomputing* 331 (2019): 50-57.
- Rezaee, Mohammad, and Daniel Letourneau. "Assessment of Image Quality and Dosimetric Performance of CT Simulators." *Journal of Medical Imaging and Radiation Sciences* (2019).
- Nancy A. Zreika, A. El-Zaart, A. Al Shakik, Toufic El Arwadi (2018), "Skin Cancer Segmentation with Entropy PAL MCET using Gaussian Distribution", 2018 4th International Conference on Applied and theoretical Computing and Communication Technology (iCATccT).
- Mehmet Sezgin and Bulent Sankur (2004), “Survey over image thresholding techniques and quantitative performance evaluation,” *Journal of Electronic Imaging.*, pp. 146–168.
- P. Yin, “Multilevel Minimum Cross Entropy Threshold Selection,” Applied Mathematics and Computation(2006)- Elsevier,doi:10.1016/j.amc.2006.06.057.
- P. Henden, “Exercise in Computer Vision - A Comparison of Thresholding Methods,” Program vareverkstedet org, 20 November 2004.
- AlSaeed DH, Bouridane A, ElZaart A, Sammouda R. Two modified Otsu image segmentation methods based on Lognormal and Gamma distribution models. 2012 International Conference on Information Technology and e-Services. IEEE; 2012: 1-5.
- ISIC2017: https://challenge.kitware.com/#phase/5840f53ccad3a51cc66c8dab Skin Lesion Analysis Towards Melanoma Detection
- Al-Attas, R., “Multi-Level Minimum Cross Entropy Thresholding Using Gamma Distribution”, Master Thesis, Department of Computer Science, King Saud University, Riyadh, Kingdom of Saudi Arabia, February, 2007.
- Al-Osaimi, G., El-Zaart, A., “Minimum Cross Entropy for SAR Images Thresholding”, IEEE International Conference on Information & Communication Technologies: from Theory to Applications - ICTTA’08, Damascus, Syria, 2008.
- Al-Osaimi, G., El-Zaart, A., “An Iterative Algorithm for Thresholding of SAR Images Using Gamma Distribution”, International Journal for Remote Sensing, 2008.
- El-Zaart, A., "A Synthetic Aperture Radar Images Segmentation Using Minimum Cross Entropy With Gamma Distribution", Signal & Image Processing : An International Journal (SIPIJ) Vol.6, No.4, August 2015.
- C. Forbes, et al.(2011), "Statsitical Distributions" 4th edition, John wiley & Sons.
- G.McPherson (1990),”Statistics in scientific investigation: its basis, application and interpretation”, Springer-Verlag.
- Li, Chun Hung, and C. K. Lee. "Minimum cross entropy thresholding." *Pattern recognition* 26.4 (1993): 617-625.
- A. W. Kopf, *et al.(1994)*, “Techniques of cutaneous examination for the detection of skin cancer”, *Cancer Supplement*, Vol. 75(2), pp. 684-690.
- D. L. Pham, C. Xu, and J. L. Prince (2000), “A survey of current methods in medical image segmentation”, *In Annual Review of Biomedical Engineering*, pp. 318–338.

- M.D. Levine and A.M. Nazif. Dynamic measurement of computer generated image segmentations. Pattern Analysis and Machine Intelligence, IEEE Transactions on, (2): 155–164, 1985.
- Oliva D, Hinojosa S, Osuna-Enciso V, Cuevas E, P_erez-Cisneros M, Sanchez-Ante G. Image segmentation by minimum cross entropy using evolutionary methods. Soft Comput. 2019; 23(2): 431-50.
- Chakraborty R, Rama Sushil R, Garg ML. An improved PSO-based multilevel image segmentation technique using minimum cross-entropy thresholding. Arabian J Sci Eng. 2019; 44(4): 3005-20.
- Kau T, Singh Saini B, Gupta S. Optimization techniques for the multilevel thresholding of the medical images. Medical Data Security for Bioengineers. IGI Global. 2019: 166-84.
- Azmat S, Wills L, Wills S. Parallelizing multimodal background modeling on a low-power integrated GPU. J Signal Process Syst. 2017; 88(1): 43-53.
- Hwang K, Jotwani N. Advanced computer architecture, 3e. McGraw-Hill Education; 2016.